NOTICE

The invention disclosed in this document resulted from research in aeronautical and space activities performed under programs of the National Aeronautics and Space Administration. The invention is owned by NASA and is, therefore, available for licensing in accordance with the patent licensing regulations applicable to U.S. Government-owned inventions (37 CFR 404, 1 et seq.).

To encourage commercial utilization of NASA-owned inventions, it is NASA policy to grant licenses to commercial concerns. Although NASA encourages nonexclusive licensing to promote competition and achieve the widest possible utilization, NASA will provide the necessary incentive to the licensee to achieve early practical application of the invention.

Address inquiries and all applications for license(s) for this invention to the NASA Management Office-JPL, 4800 Oak Grove Drive, Mail Station 180-801, Pasadena, CA 91109.

Pn .
/1) -'74
4//71
P-67

Serial No.: 08/372,640

Filed: January 12, 1995   JPL

(NASA-Case-NPO-18518-1-CU)   N95-26894
SOLID-STATE IMAGE SENSOR WITH
FOCAL-PLANE DIGITAL PHOTON-COUNTING
PIXEL ARRAY Patent Application   Unclas
(NASA. Pasadena Office) 67 p

G3/74 0049671

SOLID-STATE IMAGE SENSOR WITH FOCAL-PLANE DIGITAL PHOTON-COUNTING PIXEL ARRAY

Inventors: Eric R. Fossum
              Bedabrata Pain

Contractor: Jet Propulsion Laboratory

JPL Case No. 18518
NASA Case No. 18518-1-CU

January 12, 1995

AWARDS ABSTRACT

The invention relates to a solid-state photon-counting imaging device for low light level imaging with photoelectron counting CMOS readout of photon flux rate that features higher photon count rates than microchannel plate (MCP) imaging devices.

FIGs. 1a and 1b illustrate two embodiments of the imaging device comprising a layer 10 having a readout circuit for each of NxN photodetectors in a focal-plane array which includes a high gain, low power buffer amplifier with 1/f noise dimension and a digital counter as a unit cell. In FIG. 1a a planar layer 13 of photosensitive material having a focal-plane array 12 of NxN photodetector diodes, each diode having a free terminal and a second terminal that is connected to a second terminal of every other photodetector diode in said focal-plane array, is bump-bonded onto the silicon layer 10 having the readout circuit as shown in FIG. 2. Other techniques for bonding the layers 10 and 13 may be employed with interconnection of photodetector diodes and the CMOS circuitry as disclosed in U.S. Patent No. 5,236,871. Thus, each buffer amplifier has an input terminal directly connected to a free terminal of a separate photodetector diode for producing in response to each photon received a signal to be counted by a separate one of an NxN array or a linear array of N time shared digital counters for separately integrating over a fixed interval of time photon-produced signals received from each photodetector diode as a measurement of photon flux rate on each of said photodetector diodes of said array. In FIG. 1b the PIN photodetector diodes are interspersed in the CMOS readout circuitry, such as adjacent the NxN array of buffer amplifiers for the photodetector diodes of the NxN focal plane array, with a counter adjacent each amplifier or one row of counters time shared with every row of amplifiers.

FIG. 3a illustrates a schematic diagram for the implementation of a readout circuit for use in either monolithic or hybrid focal-plane arrays comprising a high gain, low power amplifier and two timing switches. FIG. 3b illustrates the readout circuit of FIG. 3a with a feedback capacitance for improving the readout circuit performance, FIG. 3c is a timing diagram for initial reset and then readout operation of the buffer amplifiers for the detectors of FIGs. 3a and 3b in the focal-plane imaging array of FIG. 1a or 1b. FIG. 3d illustrates schematically a technique for reducing feedback capacitance in the operational amplifier circuit of FIG. 3b by the use of a capacitive divider.

FIG. 4a illustrates a schematic diagram of a buffered direct-injection pixel readout circuit, and FIG. 4b illustrates a schematic diagram of a capacitive transimpedance amplifier (CTIA) for the readout circuit of FIG.

4a. **FIG. 4c** is a small signal equivalent circuit diagram of the CTIA of **FIG. 4b**, and **FIG. 4d** illustrates a schematic diagram of a voltage-mode background suppressed pixel readout circuit for use in a focal-plane array of **FIG. 1a** or **1b**.

FIG. 5a illustrates a schematic diagram of a current-mode background-suppressing CTIA pixel readout circuit, **FIG. 5b** shows an equivalent circuit of the photodetector in **FIG. 1b**, and **FIG. 5c** illustrates a schematic diagram of a simple current memory cell and its sources of error.

FIG. 6a illustrates schematically a basic self-biasing FET amplifier, and **FIG. 6b** illustrates schematically a self-biased cascade differential amplifier using the self-biasing technique of the amplifier of **FIG. 6a** for use as an alternative in the buffer amplifier of **FIG. 3a** for enhanced gain, low power and high output impedance for photoelectron detection in the focal-plane imaging array of **FIG. 1**.

FIG. 7 illustrates schematically cascaded buffer amplifiers for a pixel unit cell to drive a digital counter.

FIG. 8 illustrates a CMOS circuit diagram for self-biased amplifiers in the pixel unit cell of **FIG. 7**.

FIG. 9 illustrates a power saving scheme for the first of the two self-biased amplifiers of **FIG. 8**.

FIG. 10 illustrates a CMOS circuit diagram for a self-biased, high gain buffer amplifier for use as the sole amplifier in **FIG. 3a** or **3b**, or as an input amplifier in the unit cell of **FIGs. 8** and **9** to drive a digital counter.

FIG. 11 illustrates schematically the architecture for addressing one row at a time of photoelectron sensor unit cells in the focal-plane array of **FIG. 1a** or **1b** and connecting them in parallel to a linear array of buffer amplifiers, one buffer amplifier for each unit cell, the outputs of which buffer amplifiers are connected to the inputs of a row of digital photoelectron counters, one counter for each unit cell of the array corresponding to the row of photoelectron sensor unit cells in the focal plane, and a digital memory for storing separately every row of pixel data as it is developed and then read into the memory, thus providing frames of image data for subsequent processing and/or display.

The novelty of the invention resides in the provision of a high gain, low power 1/f noise dimension amplifier coupling the photodetector diodes to digital counters in a CMOS readout circuit in the embodiment of **FIGs. 1a** and **1b** for a monolithic structure (**FIG. 1b**) or virtually a monolithic structure (**FIG. 1b**).

SOLID-STATE IMAGE SENSOR WITH FOCAL-PLANE DIGITAL PHOTON-COUNTING PIXEL ARRAY

ORIGIN OF INVENTION

The invention described herein was made in the performance of work under a NASA contract, and is subject to the provisions of Public Law 96-517 (35 USC 202) in which the

5   contractor has elected not to retain title.

TECHNICAL FIELD

The invention relates to a solid-state imaging system having digital photon-counting pixels and readout circuitry.

BACKGROUND ART

10   The performance of focal-plane imaging arrays can be significantly enhanced through the use of on-chip signal processing. In state-of-the-art image sensors, such as CCDs, the photon flux on each pixel of an array is integrated as an analog charge.   Readout of the sensor array requires the

15   shifting of an integrated charge from each pixel to an output amplifier for conversion to a proportional voltage and finally conversion from voltage to digital signals for storage. Each of the shifting and converting steps introduces noise that degrades the output.   In harsh environments, sensor perform-

ance can be further degraded due to radiation interference during the readout process.

In a solid-state image sensor, the photon flux for each pixel could be integrated by a digital electronic counter

5   coupled to the pixels by amplifiers, as shown in U.S. Patent 4,710,817. The readout process then involves reading out digital signals that are not as susceptible to noise and radiation interference as analog signals are. Furthermore, analog-to-digital conversion would not be required, which is

10 another source of signal degradation problems. However, in the aforesaid patent, an array of avalanche photodiodes or a micro-channel plate (MCP) is required to provide an electrical signal of sufficient amplitude to drive digital counters through buffer amplifiers.

15   That architecture limits contrast in the output of the image sensor during the presence of incident photons arriving closely on individual pixels over such a short period of time that they are recorded as a single unit. Consequently, in an attempt to improve contrast, the photoelectron pulse created

20 by a group of photons arriving very close to each other in time is converted in accordance with its peak value and time duration into multiple units using a signal level detector with an analog-to-digital converter and a differentiating circuit. The differentiating circuit drives the counter to

achieve a unit count for each photoelectron signal pulse, and the level detector drives the analog-to-digital converter to inject into the counter a count proportional to photoelectron signal amplitude that is in excess of a threshold level set in

5   the level detector. That conversion is merely an approximation of the true image photon flux in that period of the pulse.

More discriminating PIN photon-flux detector arrays are commercially available for UV/visible photon-counting imaging

10   devices from Hughes Technology Center (HTC), but with analog integration and an analog multiplexer for pixel charge readout before analog-to-digital conversion. Thus, the HTC imaging device has much higher noise (>50 electron rms) than can be tolerated for many applications that require imaging opera-

15   tion under low light level conditions or under radiation sensitive conditions. For example, several scientific and commercial applications have been found to require accurate low photon flux level detection of images. These applications include astronomy and astrophysics, where infrared images of ob-

20   jects have led to discovery of several features that are hidden in other spectral bands.

Several astrophysics-missions with space-telescopes and spectrometers for IR band have been planned by the National Aeronautics and Space Administration or are already in use.

Satellites with IR detector arrays are being planned to explore temperatures in the upper atmosphere, conduct surveys of terrestrial minerals, water and agriculture, and record weather patterns.

5   Medical researchers are using IR detector arrays as tools to evaluate skin diseases, circulatory and neurological disorders, breast cancer and neo-natal birth. IR detector arrays also have potential applications in industrial robotics, and are being used for industrial thermography (mechanical and

10   electrical fault detection), high temperature and chemical process monitoring, spectroscopy, and materials research.

Because of these examples requiring low photon flux level detection of images, reference will sometimes be to an infrared focal-plane array (IRFPA) in the description of preferred

15   embodiments of the present invention. However, other applications require sensitive UV/visible detector arrays. Consequently, it is not intended that the concept of the invention be limited to infrared radiation bands, and for "IR" in IRFPA, "UV/visible" is to be appropriately assumed equivalent depend-

20   ing upon the context where it is used. Similarly, wherever FPA is used the reference is to be understood to be generic to IR and UV/visible focal-plane arrays (FPAs) since application of the present invention to image detection in other wavelength bands, particularly in low image intensity applica-

tions, would merely require the proper selection of the photoelectric conversion material to be used in the pixel array at the focal plane of an optical lens for the wavelength band of interest.

5   In the past, IRFPAs have commonly used a two-dimensional array of solid state detectors and an optical lens for focusing the image on the focal plane of the array. The detector pixels convert the radiation into electrical analog signals, and readout circuitry multiplexes the analog signals to an

10   analog-to-digital converter for serial pixel readout.

IRFPAs can be used in a scanning mode or a staring mode. In the early days of IRFPA radiation detection when relatively few detectors were available, the image field of the scene was mechanically scanned. However, as the IR detector technology matured,

15   it became possible to reticulate a large number of pixels with a high fill factor on the focal plane. Then the IRFPAs were operated in the staring mode. In this mode, each pixel is dedicated to detecting a very small spot of the image, thus increasing the definition of the image detected.

20   While the inclusion of a larger number of detector pixels increases the field of view, the elimination of a scanning mechanisms simplifies the system design. However, since each pixel is dedicated to a specific spot of the image, any non-uniformities of detector responsivities translate directly

into a distortion of the image. That is called detection noise. Elimination of such noise is an important design criterion for large array IRFPAs.

Like focal-plane arrays operating in UV/visible spectral bands, large IRFPAs are also required to operate with severe power dissipation, real-estate and throughput constraints. Typical dimensions of an IRFPA readout unit-cell are $50\mu m \times 50\mu m$ in area, and typical maximum power-dissipation is 100 μW/pixel. The low power-dissipation requirement also imposes a constraint on the kind of detector that can be used. State-of-the-art IR detectors are photo-conductive or photo-voltaic detectors. Photo-conductive detectors require a quiescent-current for operation, increasing the focal-plane power-dissipation. On the other hand, a photo-voltaic detector is essentially a reverse-biased diode requiring very low quiescent-current for operation. Consequently, for low-power, staring focal-plane arrays, a photovoltaic detector is preferred.

The focal-plane array throughput is dependent both on the IRFPA format as well as the application. In commercial applications, requiring real-time or near real-time decision making, the throughput requirement is high and can pose a potential problem for FPA design. However, throughput is usually not a concern in scientific applications.

There are two major differences between UV/visible and infrared imaging focal-plane arrays. First, silicon, the most familiar and best understood photoelectron conversion material, cannot be easily used for detection of infrared radia-

5   tion. This is because silicon has a bandgap energy of 1.12 eV. Therefore, a photon whose energy is less than 1.12 eV will not generate an electron-hole pair in a silicon photo-voltaic detector, thereby preventing its use for detection of IR radiation. Thus, it can be seen that IRFPAs operating

10   at 3-5 μm and 8-12 μm bands, require detector materials having band gap energy of 0.25 eV and 0.1 eV, respectively. In the absence of silicon photo-voltaic detectors at these wave-lengths, photovoltaic detectors are built on narrow band gap materials such as IV-VI compounds (lead salts), II-VI semicon-

15   ductors (mercury salts), III-V semiconductors (indium and gallium salts). IR detectors are built on indium antimonide (InSb), a III-V compound, and mercury cadmium telluride (HgCdTe), a II-VI compound. IR detection in silicon is carried out at 3-5 μm bands by using a platinum silicide

20   (PtSi) Schottky barrier diode (SBD) fabricated in an a-Si layer.

In SBDs, internal photo-emission is responsible for exciting a photo-current across the relatively small Schottky barriers. However, the quantum efficiency of PtSi in a SBD is

extremely low, being in the range of 1-2%. The quantum efficiency can be increased somewhat by changing the thickness of PtSi or by using an alternate metal film such as Pd_2Si. However, the dark-current is also increased as a result, often

5   resulting in degradation of performance rather than an improvement. Other novel IR detector technologies exist, but they are constrained by the absence of efficient low-noise readout and multiplexer structures.

Apart from the problems caused by the unreliability of

10   the photoelectron conversion materials, the reduced bandgap energy required for detection of infrared radiation also degrades the photon detector performance, because the reverse-bias current in photo-voltaic detectors depends exponentially on the bandgap energy, causing a reduction in the detector re-

15   sistance. Further, due to materials problems, IR photodetectors exhibit higher degree of response nonlinearity, poor saturation characteristics and higher 1/f noise. These problems can be ameliorated by operating the diode at a minimal reverse bias and reducing operating temperature. It is noted

20   that the zero reverse-bias operation necessarily translates to a smaller detector resistance.

The performance of IR detectors is characterized by the product of the detector area, **A**, and the zero-bias resistance, **R_o**. For the reasons outlined above, this product, **R_oA**, is

highly dependent on the operating spectral band and is also found to decrease with the increase in the background flux density as well. The decrease in the detector resistance degrades the analog signal readout circuit response by making

5   it nonlinear due to loading of the readout circuit by the detector resistance.

Unlike visible light imaging, the infrared image of a typical terrestrial scene has very low contrast and has a high background pedestal. The detection of low contrast infrared

10   image in the presence of a high-background pedestal requires accurate signal processing to estimate-and-subtract the background. Furthermore, due to response nonuniformity of the detectors, the background pedestal varies from pixel-to-pixel, requiring periodic calibration of the focal-plane array for

15   estimating the background pedestal. This signal processing is usually carried out away from the focal-plane array using expensive, computation intensive, digital signal processing techniques called nonuniformity correction methods. However, it is to be noted that a high background photon flux vis-à-vis

20   the photon flux of interest is present only in terrestrial and some industrial applications where such expensive signal processing equipment may be readily provided. Scientific and astronomical applications of IR detection do not encounter this high background, but nevertheless may suffer noise pro-

blems from readout of analog signals which then require con-
version to digital signals for further processing and/or
storage.

There are three main mechanisms by which noise is
introduced in a focal-plane readout system. First is the
temporal noise present in the semiconductor devices used for
building the focal-plane array. Secondly, focal-plane arrays
exhibit fixed-pattern noise (or spatial noise) due to
nonuniformities in detector responsivities. Thirdly, even if
the first two noise mechanisms were absent, the shot noise
present in the background flux will add noise to the readout
system. This shot noise is due to statistical variations in
the background that directly translates into an uncertainty in
the number of photoelectrons generated in the focal-plane
array. If N is the average number of photoelectrons generated
in a detector by the background radiation, the uncertainty in
this average is given by

$$\overline{n_b} = \sqrt{N} \qquad\qquad (1)$$

where the over-score symbol $\overline{n_b}$ indicates temporal average.
If the IRFPA could be operated such that all other noise is
less than the shot noise due to the background radiation, the
focal-plane array is said to operate in background limited IR
performance (BLIP). The IRFPA then operates with the theore-

tically minimum possible noise, and therefore, the goal of every IRFPA is to operate at BLIP.

The first two noise mechanisms described above are not easy to suppress, and for detectors with large response non-uniformities, such as in HgCdTe focal-plane arrays, this requires expense off-chip digital nonuniformity compensation techniques. It is the intent of this invention to drastically reduce complexity, mass and power associated with the signal processing by incorporating analog buffer amplifiers and digital integration on the focal-plane array that will allow photoelectron counting so as to minimize noise problems by, for example, reducing the detector impedance, utilizing a capacitance transimpedance amplifier (CTIA) as a buffer amplifier between each pixel having only one available terminal and a digital counter for direct digital integration of photon flux by counting photoelectrons. In conjunction with that architecture, which may be monolithic or hybrid, other techniques are intended to be used for background suppressed readout of focal-plane pixel arrays as described by Bedabrata Pain in partial fulfillment of the requirements for the degree of Doctor of Philosophy in the Graduate School of Arts and Sciences at Columbia University in May 1993, and made available to the public on January 15, 1994, by UMI Disserta-

tion Services, which by this reference is incorporated herein and made a part hereof.

STATEMENT OF THE INVENTION

An object of the invention is to provide a focal-plane
5   array of NxN photosensitive diodes in a layer of photoelectric conversion material with a high percentage fill-factor and a separate buffer amplifier for each photosensitive diode, preferably a capacitive transimpedance amplifier (CTIA) or a self-cascoding field-effect transistor (SCFET), for coupling
10   each pixel of at least a row of pixels (in which case the CTIA or SCFET are time-shared with all rows of the array) to at least a row of photoelectron counters to be time-shared with all rows of pixels, and a readout multiplexer, but preferably a unit cell for each photosensitve diode comprising a buffer
15   amplifier and digital counter. All unit cells and readout circuitry are fabricated in a semiconductor layer juxtaposed with the layer of photoelectric conversion material reticulated to define the focal-plane array of pixels in the case of a hybrid focal-plane array or in the same semiconductor layer
20   of photoelectric conversion material used for the photodetector diodes, i.e., pixels of the array. A separate unit cell provided for each pixel of the array simplifies the multiplexing part of the readout circuitry, but adds to the realestate

required for NxN unit cells instead of N unit cells. In either case, VLSI readout circuitry includes high gain, low power, analog buffer amplifiers having 1/f noise reduction capability at the input terminals of the photoelectron count-

5   ers for amplifying the signals generated by photon to electron conversion in the pixels with a conversion gain in excess of $50\mu V/e$, thereby providing ultralow light sensitivity (<1000 photons/sec) driving digital photoelectron counters.

Thus, as noted above and described in more detail below,

10   a row of N counters, and even a row of N analog buffer ampli-fiers, may be time shared with all rows of the NxN pixel array in a sample and readout process of the photon flux rate of all pixels in the array. However, it should be understood that the pixels (photodetector diodes) of the array implemented as

15   PIN diodes may be distributed among CMOS buffer amplifiers and counters for a monolithic structure in a silicon substrate. In either case, monolithic or hybrid structure, a multiplexer fabricated on the same semiconductor layer as the unit cells is provided for digital readout of the counters. The need for

20   analog-to-digital conversion is thus eliminated in the digital counter integration and readout process by direct digital integration of photoelectrons to obviate noise problems in the photon flux integration process and provide radiation harden-ing by the digital counter readout process.

The novel features that are considered characteristic of this invention are set forth with particularity in the appended claims. The invention will best be understood from the following description when read in connection with the
5   accompanying drawings.

BRIEF DESCRIPTION OF THE DRAWINGS

FIG. 1a illustrates a hybrid focal-plane imaging array of pixels formed in a layer of photoelectron conversion material by reticulating the layer into rows and columns of pixels and
10   mating that layer with a silicon layer having CMOS photoelectron digital integration circuit means and digital signal readout processing circuit means prefabricated on it. **FIG. 1b** then illustrates a monolithic focal-plane imaging array of pixels dispersed among an array of CMOS buffer amplifiers for
15   a more direct connection between the photodiode and input terminals of the buffer amplifiers.

FIG. 2 illustrates in greater detail the implementation of the array of pixels in **FIG. 1** as an array of PIN photodetectors bump-bonded onto CMOS circuitry fabricated on the
20   silicon layer for separate connection of each pixel (PIN photodetector) to a unit cell comprising a CMOS high gain, low power buffer amplifier having 1/f noise reduction capability driving a CMOS digital counter.

FIG. **3a** illustrates a schematic diagram for the implementation of a readout circuit for use in either monolithic or hybrid focal-plane arrays comprising a high gain, low power amplifier and two timing switches. **FIG. 3b** illustrates the readout circuit of **FIG. 3a** with a feedback capacitance for improving the readout circuit performance, **FIG. 3c** is a timing diagram for initial reset and then readout operation of the buffer amplifiers for the detectors of **FIGs. 3a** and **3b** in the focal-plane imaging array of **FIG. 1a** or **1b**. **FIG. 3d** illustrates schematically a technique for reducing feedback capacitance in the operational amplifier circuit of **FIG. 3b** by the use of a capacitive divider.

FIG. **4a** illustrates a schematic diagram of a buffered direct-injection pixel readout circuit, and **FIG. 4b** illustrates a schematic diagram of a capacitive transimpedance amplifier (CTIA) for the readout circuit of **FIG. 4a**. **FIG. 4c** is a small signal equivalent circuit diagram of the CTIA of **FIG. 4b**, and **FIG. 4d** illustrates a schematic diagram of a voltage-mode background suppressed pixel readout circuit for use in a focal-plane array of **FIG. 1a** or **1b**.

FIG. **5a** illustrates a schematic diagram of a current-mode background-suppressing CTIA pixel readout circuit, **FIG. 5b** shows an equivalent circuit of the photodetector in **FIG. 1b**,

and **FIG. 5c** illustrates a schematic diagram of a simple current memory cell and its sources of error.

FIG. 6a illustrates schematically a basic self-biasing FET amplifier, and **FIG. 6b** illustrates schematically a self-

5   biased cascade differential amplifier using the self-biasing technique of the amplifier of **FIG. 6a** for use as an alternative in the buffer amplifier of **FIG. 3a** for enhanced gain, low power and high output impedance for photoelectron detection in the focal-plane imaging array of **FIG. 1**.

10   **FIG. 7** illustrates schematically cascaded buffer amplifiers for a pixel unit cell to drive a digital counter.

FIG. 8 illustrates a CMOS circuit diagram for self-biased amplifiers in the pixel unit cell of **FIG. 7**.

FIG. 9 illustrates a power saving scheme for the first of

15   the two self-biased amplifiers of **FIG. 8**.

FIG. 10 illustrates a CMOS circuit diagram for a self-biased, high gain buffer amplifier for use as the sole amplifier in **FIG. 3a** or **3b**, or as an input amplifier in the unit cell of **FIGs. 8** and **9** to drive a digital counter.

20   **FIG. 11** illustrates schematically the architecture for addressing one row at a time of photoelectron sensor unit cells in the focal-plane array of **FIG. 1a** or **1b** and connecting them in parallel to a linear array of buffer amplifiers, one buffer amplifier for each unit cell, the outputs of which

buffer amplifiers are connected to the inputs of a row of

digital photoelectron counters, one counter for each unit cell

of the array corresponding to the row of photoelectron sensor

unit cells in the focal plane, and a digital memory for

5   storing separately every row of pixel data as it is developed

and then read into the memory, thus providing frames of image

data for subsequent processing and/or display.

DETAILED DESCRIPTION OF THE INVENTION

Referring to **FIG. 1a**, a solid-state photon-counting imag-

10   ing device employs CMOS circuits developed on a silicon semi-

conductor layer **10** epitaxially grown on a substrate **11** for

signal processing in a focal-plane array **12** (part of which is

shown in **FIG. 2** for three pixels in a linear array) for photo-

electric conversion using a layer **13** of suitable photosensi-

15   tive material for the wavelengths of interest, such as a-Si

for UV/visible images or other material for IR images. The

image is focused on the focal-plane array **12** with an optical

lens **14**.

In this example, the photocetectors of the array **12** con-

20   sist of fully depleted PIN silicon detector reticulated into

an array of NxN pixels with 100% fill factor. CMOS circuitry

comprising unit cells (amplifiers and counters), an accumula-

tor, and addressing means for multiplexing digital pixel data

out are produced in the silicon layer **10** and connected to the

pixels of the array **12** by bump bonding as shown in **FIG. 2** or

by a method disclosed by Fossum et al. in U.S. Patent No.

5,236,871 for producing a detector array in a layer of semi-

5   conductor material and integrated pixel readout circuitry in

a separate layer of semiconductor material lifted off a sub-

strate and bonded onto the focal-plane array after which

interconnected channels are etched and plated to provide

electrical connections to the pixels of the focal-plane array.

10   The technique of bump bonding is illustrated in **FIG. 2**

for the purpose of discussion as one example of an embodiment

of the invention using as the focal-plane array a commercially

available HAC PIN detector array that is commercially avail-

able bonded to an integrated CMOS readout circuit that is

15   unique to this invention. In other words, the intent of this

invention is not to provide a bonding technique between a

focal-plane detector array and integrated CMOS readout cir-

cuitry, but rather to improve performance of the readout

circuitry of the focal-plane array, particularly where the

20   focal-plane detector array is intended for use with low levels

of image photon flux.

In applications that permit the photodetector diodes to

be fabricated in a layer of silicon together with CMOS readout

and other CMOS circuitry, the focal-plane array of NxN photo-

detector diodes may be interspersed with an array of CMOS buffer amplifiers, one diode directly connected to the input terminal of each separate one of the NxN array of buffer amplifiers, as illustrated in **FIG. 1b.** In that case, a separate

5 digital photon counter may be provided for each buffer amplifier interspersed in the focal-plane array as an integral part of each photodetector unit cell in the array, or one row of counters may be time shared with a row of photodetector diodes.

10   In either case, hybrid or monolithic focal-plane array, CMOS unit cells include at least a buffer amplifier, each row of which may timeshare N digital counters for an array of NxN pixels. Alternatively, each unit cell may include a digital counter. A digital buffer memory is separately provided

15 together with all necessary timing and control circuits for the pixel array data read out sequentially row by row from the buffer amplifiers and counters. As will become apparent from later discussion with reference to **FIG. 10** of a time-sharing architecture, the CMOS unit cells may be produced simultan-

20 eously as CMOS integrated circuitry but with the buffer memory on a part of the silicon semiconductor that extends beyond the array of NxN pixels.

     The intent of whichever fabrication method is chosen to provide a monolithic or a hybrid focal plane is to connect the

input terminal of the CMOS unit cells as directly to the one

photodetection diode terminal of each pixel as possible to

drive separate ones of the photoelectron digital counters for

unit counts in response to each photoelectron produced in the

5   respective pixels at the focal plane. Alternatively, N rows

of pixels may be read out through one row of time-shared

digital counters when only the CMOS circuit of the buffer

amplifiers fit within the pixel area, but when feasible to

include both the CMOS buffer amplifiers and CMOS digital

10   photoelectron counters of the pixel cell units within the

pixel area in order to avoid the time sharing of the one row

of counters can be avoided.

FIG. 3a illustrates the basic architecture of a high

gain, low power analog buffer amplifier 15, which may use a

15   CTIA or an SCFET amplifier to be described below, connected

directly to a terminal of a pixel detector (PIN or PN photode-

tector) 16. When the photodetector diode is fabricated in the

Si layer as a PIN diode, the CMOS circuitry may also be fabri-

cated in the same Si layer, thus providing a monolithic focal-

20   plane digital photon-counting pixel array.

Initially, a switch ϕ_{rst} is momentarily closed to reset

(discharge) the memory capacitance C_d of the photosensor.

Then after a set period of time, a switch ϕ_{col} is closed to

sample the pixel flux as shown in FIG. 3c. Each incident

photon producing a photoelectron will produce, through the high gain amplifier (conversion gain in excess of $50\mu V/e$), an amplified voltage pulse sufficient to drive a digital counter through a column bus B_c. This assumes the photodetector diode

5   16 is fabricated within the CMOS area for the amplifier 15 or is placed directly under the pixel area of that detector 16 to which it is dedicated for directly connecting the input terminal of the amplifier 15 to the single terminal of the pixel detector 16 in the case of the hybrid focal-plane array illus-

10   trated in FIGs. 1a and 2, and that the digital counter is not placed under the pixel area with the amplifier 15 but is instead located near a CMOS digital memory produced in the extended part of the silicon layer 10 and connected to it by the column bus B_c, either as one counter dedicated to one

15   pixel in the focal-plane array, which is yet another possible arrangement, or as one counter of a row of counters time shared with all rows of the focal-plane array.

In any of the three possible architectures, operation of the readout circuit is enhanced by implementing it as a

20   capacitive transimpedance amplifier (CTIA) 15′, i.e., with a feedback capacitance C_f as shown in FIG. 3b. In either case, the buffer amplifier is preferably implemented as a CMOS circuit with sufficient pulse gain to overcome distributed line capacitance C_L of the column bus to drive a counter.

After each Q_{rst} pulse discharges the capacitor C_f through a parallel switch, a timing pulse ϕ_{col} connects the buffer amplifier to the column buffer and waits for a photoelectron (indicated as a dot on the V_o output trace) to be counted.

5   The waiting period shown in **FIG. 3c** is selected to minimize the possibility of more than one photon being detected during that period, a feat made possible by designing the CTIA using CMOS circuit techniques.

It has been shown that reduction of the detector imped-
10   ance in the long wavelength IR (LWIR) spectral band (8-12 μm) is one of the two main causes of inaccurate readout of IR signals. The lowering of the zero-bias resistance (R_o) of the detector **16** makes the readout circuit of **FIG. 3b** nonlinear and causes a larger portion of the photo-current to couple into
15   the detector resistance. The proportion of the current coupled to the readout circuit depends on the ratio of the zero-bias detector resistance to the input impedance of the readout circuit, i.e., the CTIA. The problem of low detector resistance can therefore be circumvented by constructing readout
20   circuits that either reduce the input impedance of the readout amplifier, or effectively increase the detector resistance seen by the readout amplifier. One such circuit is the buffered direct-injection input amplifier stage of the readout circuit as shown in **FIG. 4a** which operates by modulating the

gate of an injection field-effect transistor (FET) M_{inj} proportional to the change in the detector bias so that the transconductance (also the input impedance of the circuit) of the injection FET increases by a factor of $(1+A_v)$, where A_v is

5   the gain of the buffer-amplifier.

In either a monolithic or hybrid focal-plane array, only one terminal of the detector is available to the readout circuit, the other terminal (V_{det}) being common to all detectors. For that reason there are only a few readout

10   circuits that can be considered for use in conjunction with detectors having a low R_oA product. If instead both the terminals were available, other alternative designs would be possible for use in the circuit of **FIG. 3a**. However, there is at least one other circuit that is compatible with such

15   detectors having a low R_oA product. This circuit, shown in **FIG. 4b** is the capacitive transimpedance amplifier (CTIA) referred to above with reference to **FIG. 3b**.

The CTIA of **FIG. 4b** is a feedback amplifier that is used to integrate the photo-current on a feedback capacitor C_f, as

20   shown in **FIG. 3b**. The circuit consists of an input network consisting of the capacitor C_d in **FIG. 3b** and the input imped-ance R_o of the amplifier **15'**; a feedback network consisting of the MOSFET-switch M_{RST} and the capacitor C_f; and a MOS differential amplifier **15"** with a differential gain of A_v.

The circuit operates as follows. Once the switch M_{RST} is closed, the amplifier functions in unity-gain-mode, so that the dc level of the output, which is tied to the inverting input, settles to a value very close to the dc bias on the

5   noninverting input V_B. The residual difference between the voltage levels of the two inputs depends on the open-loop gain of the amplifier, as well as offsets resulting from component mismatches. Having established the operating conditions, the switch M_{RST} is opened and the photo-current is allowed to inte-

10   grate on the capacitor network. The maximum integration-time is limited by the dynamic range of the amplifier. However, the presence of the resistors (comprising the detector resist-ance and resistors in the feedback loop) in the circuit fur-ther lowers the maximum possible integration-time. This can

15   be observed from the transfer function of the CTIA, which is derived from the equivalent circuit shown in **FIG. 4c** with the resultant current transfer function being given by:

$$H_i(f) = \frac{V_{out}(f)}{I_d(f)} = \frac{1}{\left(g_f + \dfrac{g_o + g_f}{A_{vo}}\right)\left(1 + j\dfrac{f}{f_c}\right)\left(1 + j\dfrac{f}{f_a}\right)} \qquad (2)$$

with the cut-off frequencies defined as:

$$2\pi f_c = \dfrac{g_f + \dfrac{g_f + g_o}{A_{vo}}}{C_f + \dfrac{C_f + C_d}{A_{vo}} + \dfrac{C_L + C_f}{A_{vd}}} \; ; \qquad A_{vo} = \dfrac{g_m}{g_{ds}} \; ; \qquad A_{vd} = \dfrac{g_m}{g_d}$$

(3)

$$2\pi f_a = 2\pi f_L A_{vo} \dfrac{1}{1 + \dfrac{C_d}{C_f}} \; ; \qquad 2\pi f_L = \dfrac{g_{ds}}{C_L + C_f}$$

The pole given by f_a is due to the differential ampli fier, and that given by f_c is due to the resistor-capacitor network at the input and in the feedback loop. It can be seen from the expression for the transfer function that the detec-

5   tor resistance has been effectively increased by a factor of A_v, the open-loop gain of the amplifier. Thus, by designing the CTIA with a high enough open-loop gain, the errors intro- duced by low R_o value can be avoided.

The cut-off frequency f_c should be much smaller than f_a

10   in order to allow proper integration of the photo-current. If this is the case, the cut-off frequency of the CTIA is deter- mined by f_c, and smaller its value, longer can be the integra- tion-time. If the bandwidth due to the input and feedback network is smaller than the MOS amplifier bandwidth, the

15   effective time-constant (τ_c) of the CTIA is determined by the resistor capacitor network at the input and the feedback loop, and can be calculated from Equation (3) to be:

$$\tau_c = \frac{C_f + \dfrac{C_d + C_f}{A_{vo}}}{g_f = \dfrac{g_d + g_f}{A_{vo}}} \qquad\qquad (4)$$

For typical values of the capacitances and resistances, τ_c is of the order of 5 msec for a LWIR detector. Since, the integration-time must be smaller than the time-constant, this means that the integration-time of a typical LWIR readout for terrestrial applications is limited to about 1 msec.

While the high background-flux in LWIR makes it possible to theoretically reach lower NEΔT levels, where NEΔT is defined as the equivalent temperature differential in the background for which the IR signal at the output of the detection system is equal to the electronic noise at the same mode, it also demands unduly large analog storage capacity. In other words, the required storage capacitor is too big to be integrated into a focal-plane array unit cell. However, if the number of the background photocharges could be estimated and subtracted at the readout unit-cell amplifier circuit, the limitation imposed by the signal handling capacity can be overcome. Additionally, such a circuit would possess several desirable features as follows:

1.   The increased electronic signal-to-background contrast (i.e. the contrast seen by the readout cir-

cuit) will ease the dynamic range requirement of
the readout circuit.

2.   Since the background-flux will, anyway, be con-
     verted into an equivalent number of charges by the
     photo-detector, it is possible to achieve a very
     low value of NEAT, in spite of the fact that the
     number background-charges at the output of the
     readout amplifier circuit is reduced to an insig-
     nificant level.

3.   Lastly, it is pointed out that background-subtrac-
     tion acts as a non-uniformity suppressor, reducing
     the spatial noise and making BLIP operation feas-
     ible even with detectors having large non-unifor-
     mity.

Voltage-mode Subtraction of Background Charges

The background-charge-estimation can be carried out
either in the voltage domain or in the current domain. In the
voltage-mode operation of the background suppression circuit,
shown schematically in **FIG. 4d**, the background-flux is esti-
mated by integrating the background-charges on the capacitance
C_1. It is subsequently sampled-and-held on capacitance C_2.

The background-pedestal, stored on C_2, is finally subtracted when the IR signal is read out, thereby canceling the background-pedestal. The subtraction can, in principle, be carried out with a differential amplifier.

Apart from the issue of signal handling capacity, one of the major problems with this scheme is the offset produced by the charge-feedthrough from the switch M_{samp} in **FIG. 4d**, and the nonuniformity in the buffer-amplifier due to threshold voltage variations. It has been shown that the feedthrough-related error is of the order of 30 mV or more for reasonably large capacitances. Further, threshold-related error can add another 15-20 mV to it. Since the minimum signal-to-background contrast is very small (0.01 or less), the random error in the background-estimation will be more than the detectable signal.

Available offset and non-uniformity free sample-and-hold circuits require the use of amplifiers and complicated clocking-schemes in order to achieve the required compensation. This results in an unacceptable increase in real-estate and power for focal-plane array applications. Alternately, the sample-and-hold circuit can be replaced by a CCD-based analog buffer memory that is small enough in size and power consumption for focal-plane array applications.

Although demonstrated to operate without offset, this CCD-based scheme was not pursued, since voltage-mode background-suppression is inherently limited by signal handling capacity.

5   Current-mode Subtraction of Background-Flux

Since the background-flux presents itself to the readout circuit in the form of a current, it is more sensible to carry out the background-subtraction in the current-mode itself. Unlike the voltage-mode operation, subtraction of the back-

10 ground-pedestal in the current-mode is carried out prior to photo-current integration, resulting in reduction of the background-current itself. Consequently, far fewer background-charges are integrated on the focal plane, resulting in over-coming charge handling capacity limitations.

15   The current-subtraction scheme can be incorporated along with the focal-plane readout circuit by adding a transistor in the feedback loop of the CTIA as shown in **FIG. 5a.** An equivalent circuit of the photodetector **16** shown in **FIG. 5a,** which is the same detector shown in **FIGs. 3a** and **3b,** is shown

20 in **FIG. 5b.** For the operation of the background-suppressed CTIA readout circuit, a calibration-cycle is needed. During the calibration-cycle, the focal-plane array is made to stare at an equivalent background-scene, and the resultant

background-current is memorized in the circuit. This is
accomplished by resetting the circuit of **FIG. 5a** by turning
the switch M_{RESET} ON. This operation biases the transistor M_{mem}
with its gate-and-drain short-circuited. The background-

5   current flowing from the detector is coupled to the transistor
M_{mem} and the gate-to-source voltage of the transistor charges
up to the required voltage level to support this current. At
the end of the calibration-cycle, the switch M_{RESET} is shut OFF,
causing a voltage to be stored on the capacitor C_{mem}, the

10 voltage being equivalent to the channel current through M_{mem}.

During the readout-phase, the detector current increases
by an amount equal to the signal current. The voltage stored
on C_{mem} causes a current to flow through M_{mem}. This current is
the same as the background-current. Thus, the share of the

15 detector current that is due to the background-flux, is
bypassed through the transistor M_{mem} and is therefore not
integrated on the capacitance C_{int}. In other words, the
background-flux is subtracted in this circuit by bypassing it
through M_{mem}.

20 The transistor M_{mem} along with the reset-switch and the
storage capacitance C_{mem} is called the current memory circuit.
Of course, due to an error associated with the current memory,
whose sources will be described later, the entire background
current is not subtracted, but is reduced to a value equal to

κI_b, where κ is the background-suppression factor and I_b is the background-current. Using the circuit shown in **FIG. 5a**, typical values Of κ have been measured to be 0.1%. By comparing **FIG. 5a** with **FIG. 3b**, it will be appreciated that the current-mode background suppressing CTIA shown in **FIG. 5a** is a preferred embodiment of the basic detector readout circuit of **FIG. 3b**.

Another parameter of concern is the injection efficiency of the circuit during calibration. It can be calculated by writing KCL at the input node of the CTIA. Noting that the impedance of the transistor **M$_{mem}$** during the calibration-phase is equal to its transconductance (g_m), the injection efficiency (in the calibration-phase) can be computed as:

$$\eta_c = \frac{i_{M_{mem}}}{i_p} = \frac{g_m R_o (1 + A_{vo})}{1 + g_m R_o (1 + A_{vo})} \qquad (5)$$

For typical values in LWIR, such as R_o = 0.5 MΩ, gm = 1 μA/V (for I_b = 100 nA) and A_{vo} = 200, Ω_c=0.99.

One advantage of using the circuit of **FIG. 5a** over a buffered direct-injection circuit is that unlike the latter, the circuit of **FIG. 5a** is not susceptible to injection efficiency (η) degradation during the integration-mode. As long as the integration-time (T_{int}) is smaller than the time-

constant (τ_c) of the circuit, the impedance of the capacitors

is much more than that of the resistors during integration,

and all the detector current is coupled into the capacitors

only. Of course, during integration, the photo-current is

5   shared between capacitors C_{int} and C_d. However, this does not

degrade the performance of the readout circuit, since unlike

the detector resistance, the detector capacitance C_d does not

depend upon the background flux. Further, due to the feedback

operation, the detector capacitance is effectively reduced by

10   a factor of A_v compared to C_{int}, in a manner similar to im-

provement in injection efficiency. The performance of this

background-suppressed readout circuit depends upon the

performance of the current memory portion of the circuit which

will now be discussed.

15   <u>Current Memory</u>

MOS transistors require no gate current to control their

drain currents. Dynamic analog techniques have exploited this

property for storage of analog information on the gate

capacitor. These techniques have often been used for offset-

20   compensation and proper biasing of CMOS amplifiers. In recent

years, current-mode analog signal processing has been shown to

perform better than voltage or charge-mode signal processing

in some applications. Consequently, sampled-data systems have tried to tap the advantages offered by current-mode analog signal processing by developing sampled-current techniques. Current memory is an example of a sampled-current circuit. It
5   is essentially a sample-and-hold cell, as illustrated in **FIG. 5c** which indirectly samples the drain current flowing through a MOSFET by storing its gate-to-source voltage required to maintain that current.

This circuit has been referred in literature by various
10   terms such as current copier cell, current self-calibration circuit, and dynamic current mirror. The operation of the circuit can be understood from the simple circuit diagram shown in **FIG. 5c**. The current Q_{feed} to be memorized is made to flow through the memorizing transistor M_{mem} when the clock ϕ_{wrt}
15   is high by short-circuiting the gate and the drain of the memorizing transistor. The short-circuiting is achieved by turning ON the MOSFET switch M_{sw} when ϕ_{mem} is high. The gate voltage of the memorizing transistor M_{mem} is charged up to an adequate level required to support the drain current. After
20   the switch M_{sw} is turned OFF, this voltage is held on by the capacitor C_{store}, so that at a later time, when the clock ϕ_{read} goes HIGH, memorized current is read out.

The current memory system is affected by parasitic capacitance C_{par} in the store and readout circuit as will be noted below.

Since the same transistor is used both to read and write data in the current memory, the very notion of mismatch due to technological variations disappears. This is unlike circuits operated in voltage-mode, where cell-to-cell mismatch is a major source of random error. However, a current memory has its own sources of error, the main one usually being the charge-feedthrough associated with the MOSFET switch M_{mem}, causing the sampled voltage to be different from the actual gate-to-source voltage of the MOSFET.

The current retrieved from the current memory will always be different from the current that was memorized by a small amount. For a current memory array, two kinds of errors are of concern, the original-to-copy error and the relative error. The original-to-copy error refers to the error (within a given cell) between the current memorized and that read out. The sources of this kind of error are indicated in **FIG. 5c.** The relative error refers to the fractional difference in the current read out from two different current memory cells, after the same current was written into both of them.

The main source of error in a current memory is the switch-feedthrough. Switch feedthrough refers to the residual

channel-charge of a MOSFET-switch that is dumped on the stor-
age node following the turn-OFF of the MOSFET. If Q_{ch} be the
channel charge present under the MOSFET gate when it was ON,
and C_{store} be the storage capacitance, the switch-feedthrough is
5   given by:

$$\frac{\Delta I_{ft}}{I} = \frac{g_{mm}Q_{ch}}{C_{store}} \qquad\qquad (6)$$

Since the switch-feedthrough-related error depends upon the
g_m/I ratio, the fractional error given by the Equation 2 is
lower for higher values of current memorized, i.e. when the
transistor operates in strong-inversion. This is because in
10   strong-inversion, g_m is proportional to the square root of the
drain current. Therefore, g_m to I ratio, decreases with in-
creasing levels of current memorized, thereby reducing the
fractional error. On the other hand, when extremely small
current-levels (1-200 nA) are memorized, causing the memoriz-
15   ing transistor to operate in weak-inversion, the transconduct-
ance can be expressed as:

$$g_m = \frac{I}{mV_{kT}} \qquad\qquad (7)$$

where m is a constant that varies from one transistor to

another.   Its typical value is between 3 to 5 for CMOS

technology.   Equation 2 can now be rewritten as:

$$\Delta \frac{I_{ft}}{I} = \frac{Q_{ch}}{mV_{kT}C_{store}} \tag{8}$$

The switch-feedthrough error is independent of current for the

transistor operating in weak-inversion and is inversely pro-

5   portional to the storage capacitance size.   For W_{sw} = 3 μm, L_{sw}

= 5 μm, C_{ox} = 0.85 fF/μm^2, V_{gs} - V_T = 1V, and C_{store} = 0.5 pF, the

charge feedthrough-related error can be calculated from Equa-

tion (8) and is of the order of 25%, if it is assumed that the

channel-charge is split in equal halves, and one half goes to

10   the drain side and one half to the source side.

The actual charge that is fed onto the source end depends

upon a number of factors.   It has been shown that the charge-

feedthrough depends upon the rate of turn OFF of the MOS

switch, its ON conductance, the impedance on the drain end,

15   and the ratio of the capacitance on the drain to that on the

source side.   For a slow enough rate of switch turn-OFF, the

fraction of channel-charge fed through to the source side

becomes smaller as the ratio of the drain side capacitance to

the source side capacitance decreases.   For a current memory,

20   the source-end capacitance (C_{store}) is less than that in the

drain-end (C_{load}, not shown).   Therefore, for slow enough turn-

OFF rate, the amount of switch feedthrough to the storage node
decreases.   Even then,   the   resultant   switch   feedthrough-
related error can be significantly large.

5   The drain-to-source voltage of the memorizing transistor
during   the   write-mode   is   the   same   as   its   gate-to-source
voltage.   However, in the readout-mode, this voltage will be
larger causing the current flowing through the transistor to
be different due to the finite output impedance of a MOSFET in
saturation.

10   The   small-signal   output   conductance   of   a   MOSFET   in
saturation is dependent on the current flowing through it, and
is usually modeled as:

$$g_{ds} = \lambda I_{ds} \tag{9}$$

with values of λ being in the range of 0.01 to 0.05 for a 2 μm
15   CMOS technology.   Further, the output conductance is more for
a p-MOS than for an n-MOS by a factor as much as 5 times.   The
error   induced   by   the   channel-length-modulation   can   be
expressed as:

$$\frac{\Delta I_{cl}}{I} = \frac{g_{ds}\Delta V_{out}}{I} = \lambda\Delta V_{out} \tag{10}$$

This error is also independent of the current memorized and is of the order of 2-5%.

There is always a parasitic capacitance (C_{par}) between the drain and the gate of a MOSFET, a large component of which is the overlap capacitance between the gate and drain. This overlap capacitance C_{gd} is proportional to the width of the memorizing transistor M_{mem} and is usually small. However, when the stored memory is being read out and the drain voltage is different from what it was during the write-phase, this capacitor C_{par} will couple a part of this increased drain voltage to the gate, causing a change in the current proportional to the increase in the drain voltage. This error can therefore be expressed as:

$$\frac{\Delta I_{cc}}{I} = \left(\frac{C_{par}}{C_{par} + C_{store}} \right) \frac{\Delta V_{out}}{mV_{kT}} \tag{11}$$

where V_{kT} is the thermal voltage. Equation (11) indicates that the error can be kept small by reducing the parasitic capacitance, and by making the memorizing capacitance C_{store} large which can be done by proper integrated circuit layout. Temporal errors in a current memory are caused when the write-time is too small or when there is junction leakage associated with the memorizing node between the switch M_{sw} and the capacitance C_{store}. If the write-cycle is terminated before

the circuit settles in equilibrium, and the gate voltage of
the memorizing transistor cannot charge up to its proper
value, there will be an error during the readout-phase. This
error is particularly troublesome for small currents memor-

5   ized, since for small currents the memorization time is usual-
ly longer. The memorization time is mainly determined by the
time-constant due to the C_{store} and the transconductance of the
memorizing transistor C_{mem}, since the switch ON conductance is
much larger than the transconductance (g_m). Assuming a

10   single-pole system, the error in the gate voltage as a
function of the write-time (t_{wr}) is given by:

$$\frac{\Delta V_{gs}(t_{wr}) - V_{gs}(\infty)}{V_{gs}(\infty)} = \exp\left(-\frac{t_{wr}}{\tau_{mem}}\right) \tag{12}$$

where τ_{mem} is memorization-time-constant given by:

$$\tau_{mem} = C_{store}/g_{mm} \tag{13}$$

It can be seen from Equation (13) that the smaller the current
the larger the memorization-time-constant. Since a small

15   error in the gate voltage causes a large error in the drain
current, $t_{wr} > 10 \cdot \tau_{mem}$, for this error to be negligible.

The other temporal error is caused by the p-n junction-
diode leakage at the memorizing node. The presence of this

error cannot be avoided since the source of the switching transistor M_{sw} is connected to this node by this diode. The leakage-current associated with this diode will decrease the voltage on the capacitance C_{store}, so that the memory perfor-

5   mance will degrade over a period of time. The time duration over which the memory is retained depends upon the tolerable error and the magnitude of the leakage current. This error can be expressed as:

$$\frac{\Delta I_1 k}{I} = \frac{g_{mm} I_1 \Delta t}{C_{store} I} = \frac{I_1 \Delta t}{m V_{kT} C_{store}} \qquad (14)$$

The noise associated with the circuit MOSFETs will impose

10   a physical limit to the minimum error level that can be reached by the current memory even if all other sources of error were suppressed. However, at present, current memory operation is far from being limited by noise. The noise in current memory is contributed from two other distinct sources.

15   First, there is a statistical uncertainty in the voltage sampled on C_{store} following the shut-OFF of the switching transistor. This uncertainty is due to the sampling of the noise of both the MOSFETs M_{sw} and M_{mem}. This noise is called the reset-noise, and is present in any circuit that operates with peri-

20   odic-reset. The noise due to the switch is negligible, where-

as the noise in memorizing MOSFET determines the reset noise and the uncertainty in the voltage sampled is given by:

$$\overline{V_n^2} = \frac{kT}{C_{store}} \tag{15}$$

Further, during the readout of the current memory, the channel noise is also present and causes another error in the memorized current. At the same time, because of the periodic

5   reset of the circuit, it reduces the low-frequency 1/f noise of the current memory.

When the CMOS counters will not fit under the limited pixel areas with its cell unit, a row of N photoelectron

10 counters may be produced on the extended silicon semiconductor area together with the digital memory, one digital counter for each column of the NxN pixel array, each to be time shared by all N pixels in the column. As these N digital counters complete sampling a row of N pixels over a timed integration

15 period, the contents of the counters are transferred serially or in parallel to a corresponding row of N registers in the digital memory. The necessary address decoding and timing circuits are also produced on that extended silicon semiconductor area. In an extreme case of very high definition, it

20 may be necessary to place even the unit cell amplifier for each of the pixels in the extended part of the silicon

semiconductor layer next to the digital converters. In that case, only N time shared unit cells are provided, one for each of N photoelectron counters for each of N columns of pixels.

Improved Readout Circuitry

5   Although the readout circuits in **FIGs**. **3a** and **3b** through **FIGs**. **5a** and **5c** may be found in the literature in other contexts, i.e., in other architectures, the following unique readout circuits will provide better performance for low light level imaging with lower voltage and power requirements in

10   either monolithic or hybrid architectures. MCP detector arrays which operate at a high voltage (2000 volts), large effective pixels (40 μm resolution), low intrinsic quantum efficiency at Lyman-α (1216Å, 8%), high sensitivity to water vapor and the need to be periodically "scrubbed" for

15   stability. CCD detector arrays offer large formats, low noise readout and do not require such high voltages, but have an equally unappealing collection of limitations. These include the need for backside illumination or frontside application of a down converting phosphor.

20   Backside illumination calls for thinning a large area device and then treating the mechanically fragile surface to ensure electrical stability and high UV QE. The use of a frontside phosphor results in more limited QE and cutoff at

about 500 Å. The high vapor pressure of the phosphor, and its tendency to crystallize leads to long term reliability concerns.

Other issues important for CCDs are their fundamental
5   sensitivity to radiation (e.g., proton) damage that signifi- cantly reduces charge transfer efficiency and hence signal fidelity, and residual read noise (3-5 e- rms) that precludes photon counting. It should also be noted that while sub- electron read noise has been demonstrated for CCDs using
10   multiple non-destructive sampling, the transport of single electrons (or even a few electrons) across macroscopic distances has not yet been demonstrated. (CTE is typically quoted for more than 1000 electrons in a charge packet, and with enough illuminated pixels to ensure that single electron
15   traps are filled.)

While both CCD and MCP approaches find supporters and continue to be improved, one would like to ideally combine the photocounting ability of the MCP detector array with the com- parative ease of solid-state monolithic detectors whenever the
20   photoelectron conversion material can also be used for the readout circuits, as in the case of CMOS circuits for PIN photodetector diodes. This is so it would be possible to have a detector array that could count photoelectrons as they are generated within the pixel so that the readout could be digi-

.

tal and hence noise free. The present invention is thus in-
tended to provide an advanced solid-state monolithic photon-
counting imaging device when possible that represents a next-
generation sensor beyond the microchannel plate (MCP) device.

5   The monolithic device is a focal-plane array that
consists of a fully-depleted PIN silicon detector array with
100% fill-factor and high QE, made possible by a
photoelectron-counting silicon CMOS readout with a multi-
plexer. The purpose of this device is to count individual
10   photoelectrons on the focal plane at a much higher rate than
is presently possible with the MCP/MAMA or strip and wedge
readout system (~1000 counts/pixel/sec) with higher spatial
resolution and low voltage operation. The device will have a
25 micron spatial resolution, and quantum efficiency and dark
15   current similar to that of backside illuminated CCDs (QE $\geq$ 20%
at 100-400 nm, dark current of 40 counts/pixel/sec at -50°C).

        The array format may be readily provided with a 1024x1024
pixel array based on proven infrared hybrid focal-plane array
technology. Its main advantage is that the device will not
20   require high voltages typical of MCPs, thus simplifying
associated electronics and packaging. The size of the pixel
will scale with commercial microelectronics minimum feature
sizes and thus will have even higher resolution in succeeding
generations. Since the readout multiplexer uses the common

CMOS fabrication process widely used in space applications, the radiation hardening of the multiplexer to levels that are orders of magnitude greater than that of the CCD is also readily achievable.

5   The open-face nature of the PIN focal-plane detector array permits inclusion of UV QE enhancement technology under development for backside illuminated CCDs (e.g., various pinning technologies, down-converting phosphors, molecular beam epitaxy of thin silicon films, etc.), and will hence
10   always have a QE equal to that of backside illuminated CCDS. Thus, this invention sets the stage for a new class of UV/visible detectors that will compete favorably against the MCP technology as well as small format ($\leq 1024^2$) CCDS, especially under low light level conditions. The detectors will be
15   applicable to a wide range of future UV/visible image detectors for large and small missions.

The critical component of the improved device is the photoelectron-counting readout unit cell design. PIN detector arrays are already commercially available from Hughes Techno-
20   logy Center (HTC) as noted hereinbefore, albeit with a analog multiplexer that has much higher noise (>50 electrons rms), which lends itself to a hybrid architecture, but which is more advantageously used in a monolithic solid-state architecture. Thus, in either architecture the primary novelty of the

present invention is the photoelectron-counting circuitry.
The proposed unit cell contains a ultra-low power (<1 μW),
very high gain amplifier (A>200,000) with an embedded 1/f
noise reduction scheme that extensive circuit analysis and

5   simulation has already shown to exhibit sub-electron input-
referred noise levels. This unit cell gives high confidence
that a photoelectron counting circuit can be achieved in
minimal pixel area.

Referring to **FIGs**. 1 and **1b**, which show the photons are

10   incident on the front surface where they are converted to
electron-hole pairs through the photo-absorption process. The
electrons diffuse through the thin, neutral p-region of the
PIN photodetector diodes and enter the electric field region
(I-layer). They drift through the depleted I-layer and then

15   are collected in the neutral n-region.   The photoelectron
charges the capacitance of the buffer amplifier that includes
the detector capacitance as well as the CMOS connection capa-
citance, input transistor gate capacitance, and parasitic
circuit capacitances resulting in change in input voltage to

20   a digital counter. A digital readout multiplexer out of the
counter typically consists of a source-follower amplifier and
selection transistors for gating the readout.

Infrared focal-plane arrays of the prior art use analog
CMOS readout multiplexers. Typical read noise levels for the

most advanced multiplexers (e.g., low background) are in the
range of 30-50 electrons rms, though with multiple nondestruc-
tive readout techniques, noise levels as low as 10 electrons
rms have been reported. The major source of noise is present-

5   ly believed to be random noise introduced on the focal plane
from clocking signals. The intrinsic unit cell noise is domi-
nated by MOSFET 1/f noise for low light level signal detection
involving long integration times and is of the order of 10
electrons rms. To date, there has been no report of any ana-

10   log readout system that attempts to quantify photoelectrons
within the unit cell. The overall design of a pixel unit cell
capable of detecting a single photoelectron is as follows:

1.   The required gain of the cell buffer amplifier is
approximately 200,000. The cell size, using 0.8 μm

15   design rules, is estimated to be 25 μm x 25 μm. It
is estimated the unit cell will be capable of
counting up to 1000 photoelectrons per second and
dissipate less than 1 μW of power.

2.   Assemble the unit cells in a CMOS circuitry plane

20   with an on-chip scanner and accumulator circuits
for reading out the unit cells which include a
digital counter for photon flux integration. The
single bit output of each cell buffer amplifier is

accumulated in an array of dedicated counters located adjacent to, the detector array. This counter array is then accessed to readout the photon flux detected. The output of the counter

5   array is the digital representation of the photon flux incident on each pixel.

The basis for the unit cell high gain buffer amplifier with an embedded 1/f noise rejection scheme for simultaneously achieving low noise, high gain, low power and small real

10   estate amplifier circuits is a novel self-cascoding FET (SCFET) shown in **FIG. 6a**. The SCFET is compatible with low power operations, requires virtually no extra real estate, and features high output impedance.

The amplifier should be configured to operate in sample-

15   and-subtract mode, so that the 1/f noise sample collected during the reset phase of operation is subtracted during the high gain phase, thereby directly reducing 1/f noise.

The SCFET of **FIG. 6a** is a common-gate composite transistor consisting of a cascoding transistor M_c connected

20   in series with the controlling transistor M_1. The dimensions of the two transistors are properly chosen so that the cascoding transistor M_c acts as a screen gate shielding the main transistor M_1 from all the variations at the output node, thereby increasing the output resistance. It has been

demonstrated that a twenty-fold increment in the output resistance can be achieved with ease.

A buffer amplifier and a comparator fed by the SCFET is implemented using a cascode differential amplifier as shown in

5   **FIG. 6b.** The reason for choosing the cascode differential topology is to increase gain due to cascoding, increase power supply rejection ratio due to a small common mode gain, increase output impedance due to cascoding, and provide bandwidth control by changing the bias current. For the SCFET

10   differential amplifier to be used for electron counting applications, it is required to possess self-biasing capability. Auto biasing by dynamic analog techniques will fail to work because of the high gain of the amplifier in question. The high gain of the circuit amplifies the effect

15   of any residual switch-feedthrough causing the amplifier to be driven into saturation.

The novel switch-feedthrough canceling self-biased differential cascode amplifier shown in **FIG. 6b** is preferred. In this circuit, the composite transistors M_{i1} and M_{i2} are the

20   input transistors, M_{L1} and M_{L2} are the load transistors, and M_b is the bias transistor. Because of the increased output resistance of the SCFET, the differential amplifier possesses a large gain for a single stage (~500). This value can be

further increased, if necessary, through controlled positive feedback circuitry.

The switch-feedthrough cancellation scheme takes advantage of the low common mode gain and large common mode
5   range available in differential topology. By allowing the switch feedthrough (as a result of the shutting off of the switch ϕ) to occur in common mode, its effect can be completely suppressed.

The self-biasing action also results in 1/f noise
10   reduction due to the sample-and-subtract operation inherent in it. The noise analysis for such periodically resetting amplifiers have been carried out by the coinventor in his Ph.D. dissertation cited above and closed form expressions for noise have been derived. These closed form expressions have
15   emerged as extremely helpful tools in predicting noise performance of the 1/f noise reducing amplifier for a given bias current (I_b) and sample period (T_s). Using the results derived in the dissertation, the input-referred noise can be written as:

$$\left(\overline{v_n^2}\right)_i = \frac{\frac{4}{3}kT(g_{ml}+g_{mL})}{g_{ml}^2}\pi f_c + \frac{I_b}{g_{ml}^2}\left(\frac{K_{fp}}{L_l^2}+\frac{K_{fn}}{L_L^2}\right)\left[\ln\left(\frac{T_s}{2t_r}\right)+1.85\right]$$

$$\text{(16)}$$

$$=2kT\frac{\left(1+\frac{g_{mL}}{g_{ml}}\right)}{t_r\sqrt{2\mu_1 C_{ox}\frac{W_l}{L_l}I_b}} + \frac{1}{C_{ox}\mu_1\frac{W_l}{L_l}}\left(\frac{K_{fp}}{L_l^2}+\frac{K_{fn}}{L_L^2}\right)\left[\ln\left(\frac{T_s}{2t_r}\right)+1.85\right]$$

where g_{ml} and g_{mL} are the transconductances of the input and

the load FETS, f_c is the cut-off frequency of the amplifier,

L_1 and L_2 are the channel lengths, t_r is the response time, μ

is the mobility, C_{ox} is the oxide capacitance per unit area,

5   and K_{fp} and K_{fn} are the flicker noise coefficients. This

design equation allows the choice of an optimum channel length

and width for maximizing the signal-to-noise ratio.

Since the proposed circuit operates by counting single

photoelectrons, the dynamic range is determined by the

10   shortest and the longest possible wait times (i.e. the time

interval between the arrival of consecutive photons) of the

circuit. The maximum wait-time is determined by the tolerable

1/f noise. From Equation (16), it can be seen that the 1/f

noise depends on the ratio between the sample-period (T_s) and

15   the response-time (t_r). Since, the response time cannot be

increased beyond 0.5 msec without paying severe penalty in

terms of load capacitance size, $T_s/2t_r$ ratio can be as high as

10,000 for ultra-low level signal-detection. From Equation (16), the increase in the rms 1/f noise voltage is found to be only one-and-half times, which means that even for extremely long wait times, 1/f noise will not be critically large. The

5   shortest possible wait time, on the other hand, is determined by the tolerable white noise. It has been demonstrated that sub-electron input-referred noise is achieved over a large range of response time values. Further, there exists a trade off between the minimum response time for which single

10   electron detection is possible and the power budget. A typical number for the minimum response time is about 50 μsec, indicating that the dynamic range is more than 50,000 and the maximum count rate is greater than 1000 per pixel per sec., which is orders of magnitude higher than what is achievable

15   with MCPS.

FIG. 7 illustrates the manner in which the buffer amplifier described with reference to FIGs. 6a and 6b may be employed to implement the readout circuit of FIG. 3a using two buffer amplifiers in cascade for sensitivity given by

$$\Delta V_o = \frac{A_1 A_2 \Delta_q}{C_d} \approx 10 mV \qquad (17)$$

$$\text{for} \quad C_d = 40fF$$

$$A_1 = A_2 = 50$$

ϕ_{rst1} and ϕ_{rst2} are internal resets required for biasing the gain stages. For photon counting, neither accurate gain nor stability is required. Gain of 50-100 per stage is enough.

FIG. 8 illustrates a CMOS circuit diagram for cascaded
5   self-biased amplifiers with cascode input for reduction of Miller capacitance. Reset noise is dominated by C_1 and C_2, not by small parasitic input capacitance. Feedthrough on capacitors C_1 and C_2 limit utility for biasing the high-gain stage, with a total gain of approximately 5,000 to 10,000. However,
10   this circuit design is not unity gain stable and therefore cannot be used for the circuit of FIG. 3a.

FIG. 9 illustrates a power saving scheme for a buffer amplifier connected directly to a PIN pixel diode 16. However such a readout circuit creates some concern for parasitic
15   capacitance coupling during transition from high to low bias current and speed of switching bias currents that must be attended to in the CMOS layout.

FIG. 10 illustrates a self-biased SCFET buffer amplifier with cascode input for reduction of Miller capacitance that
20   can be used for the circuit of FIG. 3b.

FIG. 11 illustrates schematically a hybrid architecture for the readout system of FIG. 1 with an address decoder 20 for gating a unit cell buffer amplifier (CTIA or SCFET) to a row 21 of digital counters which can be serially read out if desired and an address decoder 22 for gating the time shared row of counters into discrete rows of digital registers in a buffer memory 23. This arrangement of a CMOS buffer amplifier provided in an integrated silicon chip, one buffer amplifier for each pixel in the silicon chip area underneath the focal-plane array eliminates the need for ultra-high gain buffer amplifier at each pixel, and sharing one row 21 of photoelectron digital counters provides semiparallel periodic readout, while the buffer memory 23 provides an accumulator for extended storage. A row 24 of shift registers provides ultimate semiparallel periodic readout to a permanent storage device 25, which may be, for example, a reel of magnetic tape, all under control of a programmed control unit 26.

In the event a complete unit cell comprising a buffer amplifier and a 10-bit digital counter can be integrated in CMOS circuitry in the silicon area under each reticulated pixel area, the row of counters 21 may be omitted. The decoders 20 and 22 normally coordinate control of the buffer amplifiers of the focal-plane array. Time shared counters 21 and the buffer memory 23 plus the readout shift register 24

under the control of the unit **26** would then need to coordinate the focal-plane array and counters together and the transfer of the contents of the digital counters to the buffer memory and from there to the output shift register **24** for extended

5   memory also under control of the unit **26**.

For a monolithic architecture comparable to that of the hybrid architecture in **FIG. 10,** there are virtually no constraints in the CMOS layout adopted. It would be possible to provide the SCMOS buffer amplifier and CMOS 10-bit counter

10   in a single readout cell with the PIN photodetector diode connected to the input terminal of the amplifier. Each pixel may then be read out in sequence or in parallel row by row into the buffer memory. However, it would also be possible to time share a row of digital counters as in the hybrid

15   structure. The advantage of the monolithic architecture is to be found not only in improved performance, but also in the ease of fabrication.

Although particular embodiments of the invention have been described and illustrated herein, it is recognized that

20   modifications may readily occur to those skilled in the art. Consequently it is intended that the claims be interpreted to cover such modifications and equivalents thereof.

SOLID-STATE IMAGE SENSOR WITH FOCAL-PLANE DIGITAL PHOTON-COUNTING PIXEL ARRAY

ABSTRACT OF THE DISCLOSURE

A photosensitive layer such as a-Si for a UV/visible
5   wavelength band is provided for low light level imaging with
at least a separate CMOS amplifier directly connected to each
PIN photodetector diode to provide a focal-plane array of NxN
pixels, and preferably a separate photon-counting CMOS circuit
directly connected to each CMOS amplifier, although one row of
10   counters may be time shared for reading out the photon flux
rate of each diode in the array, together with a buffer memory
for storing all rows of the NxN image frame before transfer to
suitable storage. All CMOS circuitry is preferably fabricated
in the same silicon layer as the PIN photodetector diode for
15   a monolithic structure, but when the wavelength band of inter-
est requires photosensitive material different from silicon,
the focal-plane array may be fabricated separately on a dif-
ferent semiconductor layer bump-bonded or otherwise bonded for
a virtually monolithic structure with one free terminal of
20   each diode directly connected to the input terminal of its
CMOS amplifier and digital counter for integration of the
photon flux rate at each photodetector of the array.
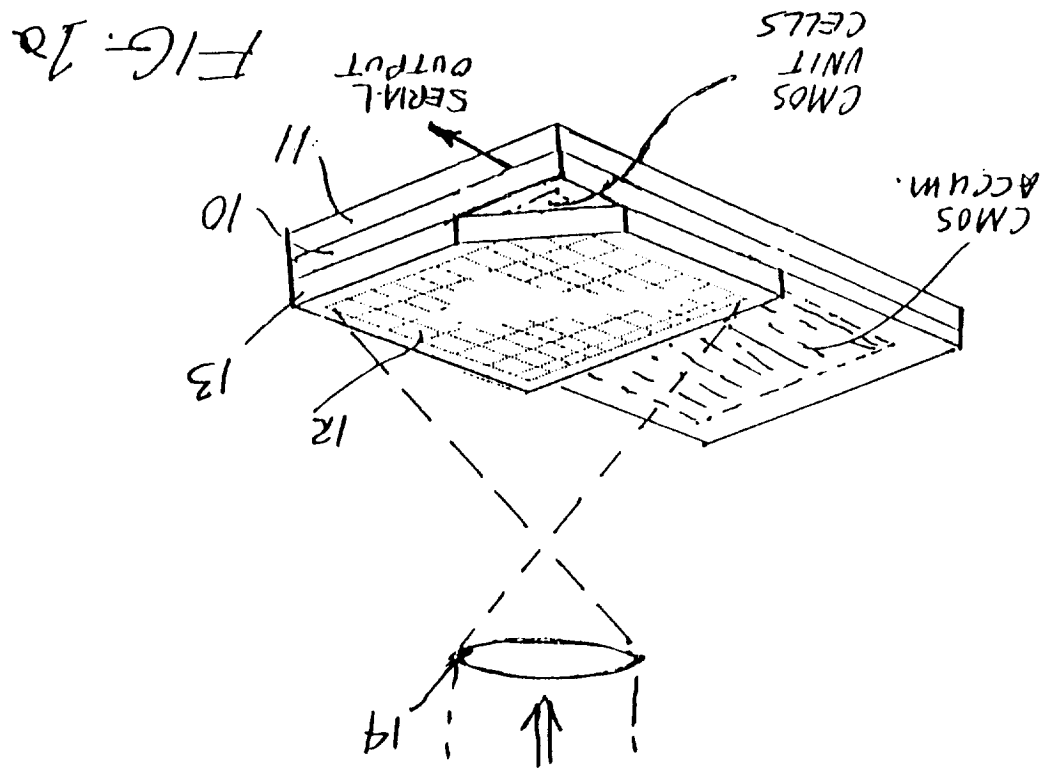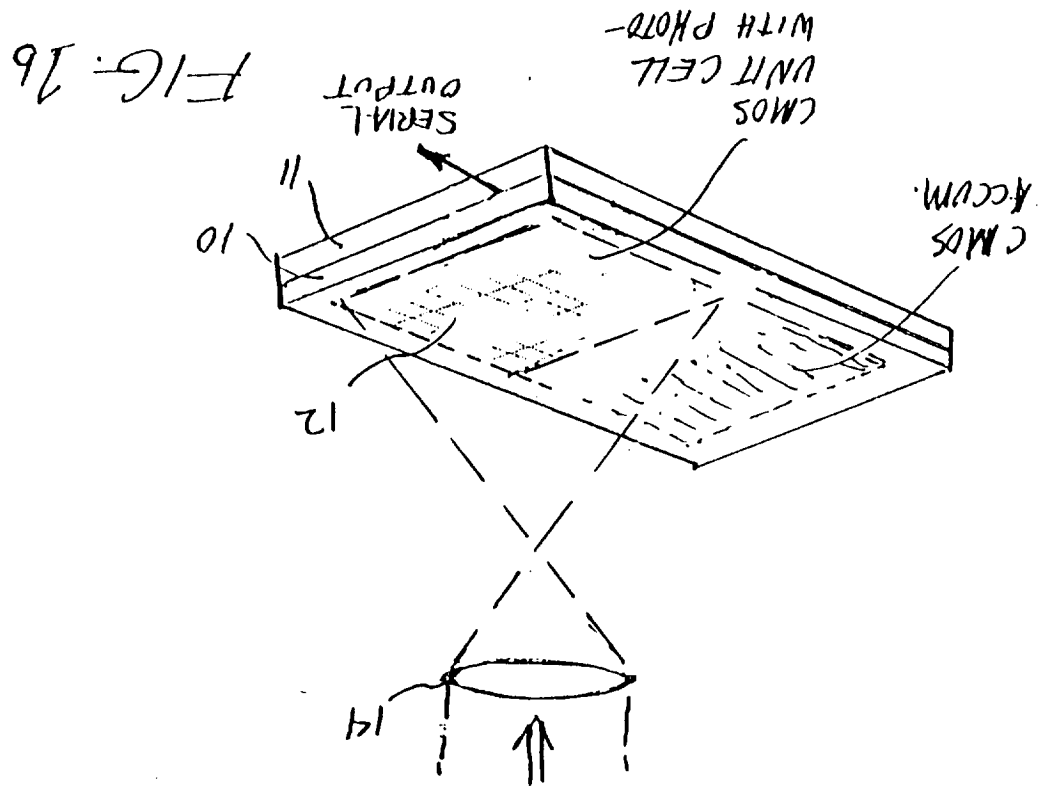
FIG. 1b

CMOS
UNIT CELL
WITH PHOTO-
ACCUM.

CMOS
UNIT
CELLS

CMOS
ACCUM.

SERIAL
OUTPUT

10

11

12

13

14

FIG. 1b

CMOS
UNIT CELL
WITH PHOTO-
ACCUM.

CMOS
ACCUM.

SERIAL
OUTPUT

10

11

12

14

NASA Case No. NPO-18518-1-CU
Page 1 of 8
SOLID-STATE IMAGE SENSOR WITH
FOCAL-PLANE DIGITAL PHOTON-
COUNTING PIXEL ARRAY
Inventor: Eric R. Fossum, et al.
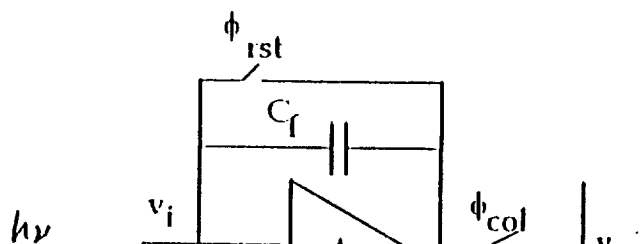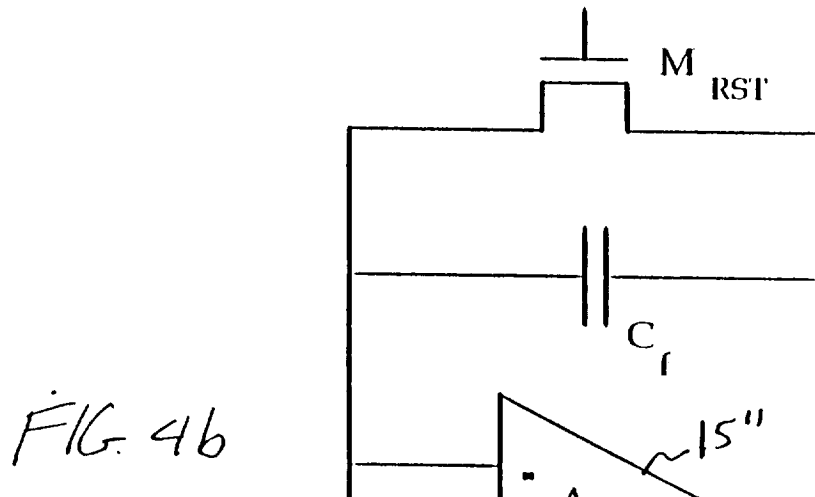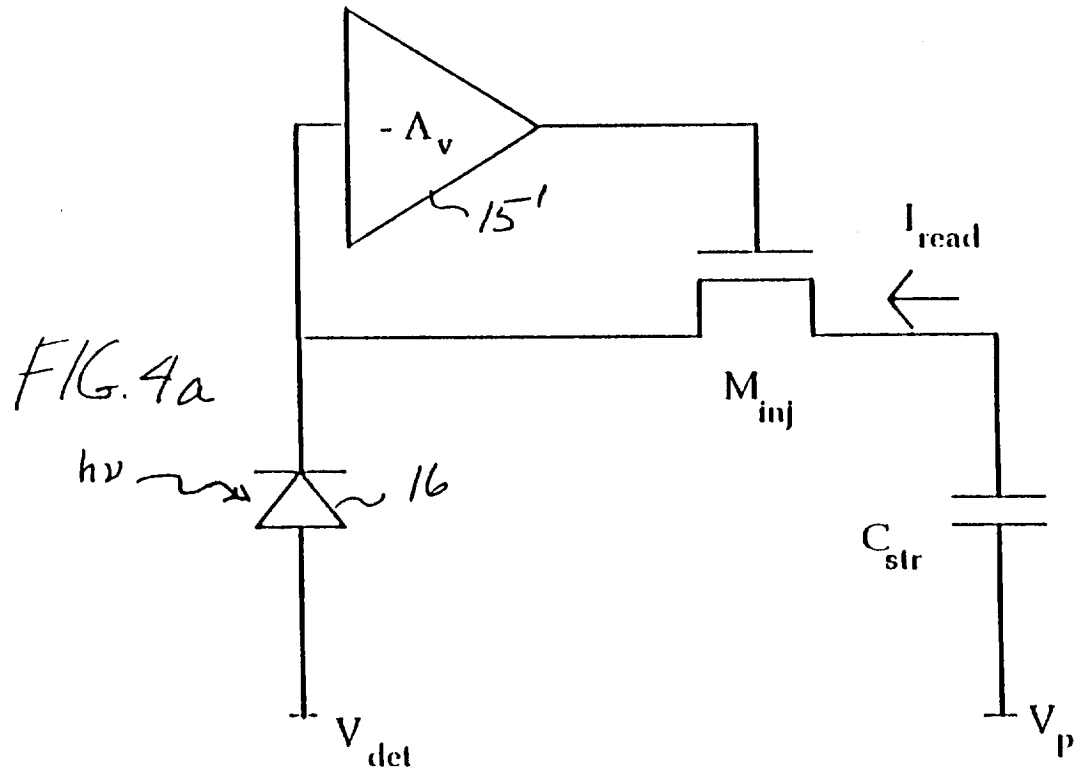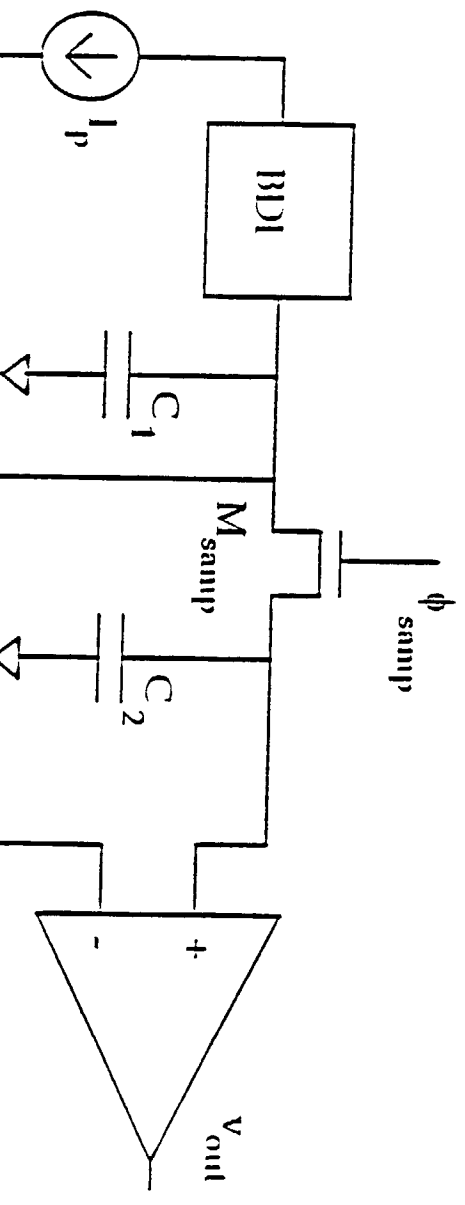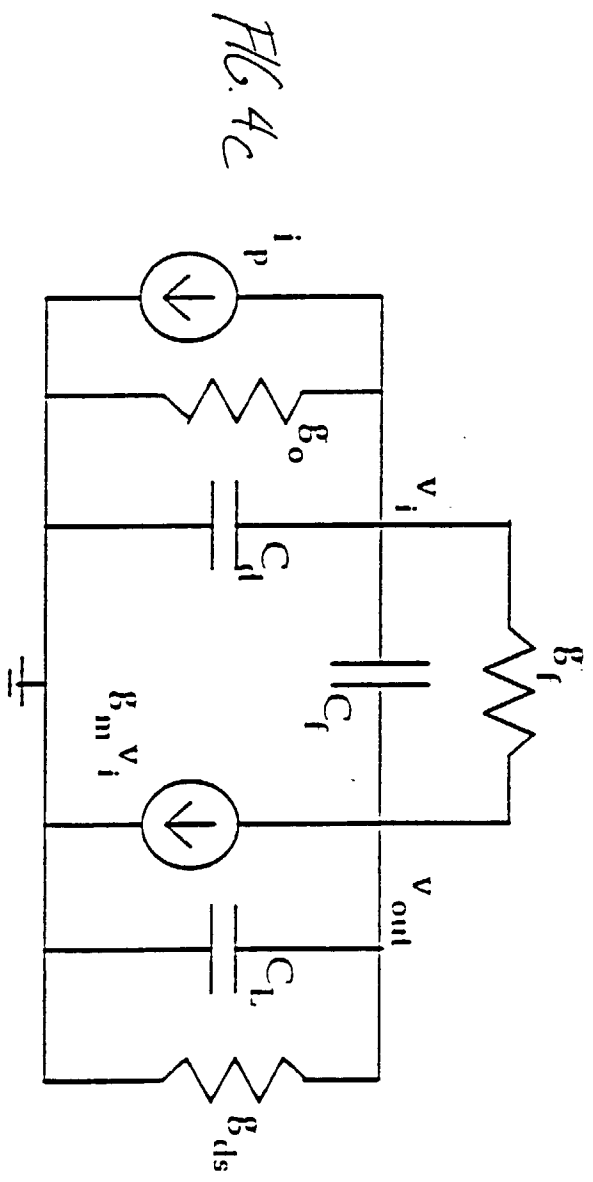
Contact: John H. Kusmiss
Telephone No. 818-354-7770

hν

PIN Detector Array

p-layer ⎫
i-layer ⎬ PHOTOSENSITIVES
n-layer ⎭ SEMICONDUCTOR

12

SERIAL
OUTPUT

CMOS CIRCUITRY | Si layer

10

FIG. 2

ϕ_{rst}

15

v_i

$-A$

ϕ_{col}

v_o

hν

16

C_d

C_L

FIG. 3a   Column Bus

ϕ_{rst}

C_f

hν

v_i

ϕ_{col}
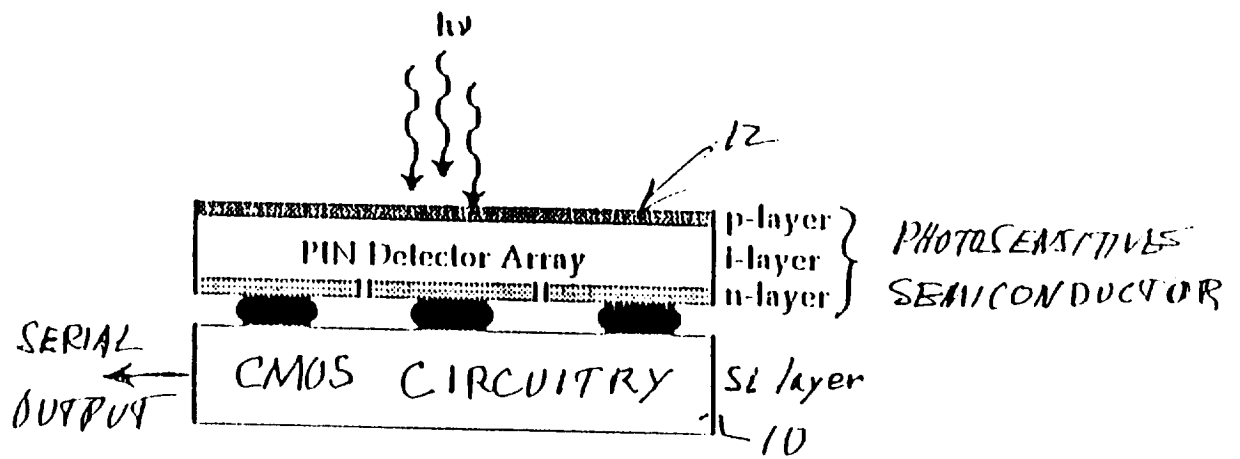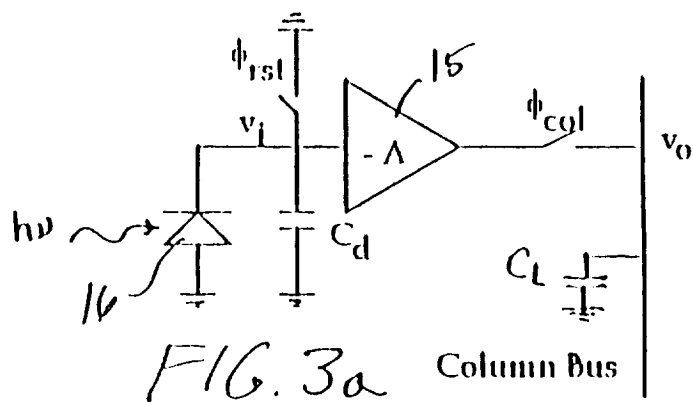
NASA Case No. NPO-18518-1-CU
Page 2 of 8
SOLID-STATE IMAGE SENSOR WITH
FOCAL-PLANE DIGITAL PHOTON-COUNTING
PIXEL ARRAY
Inventor: Eric R. Fossum, et al.

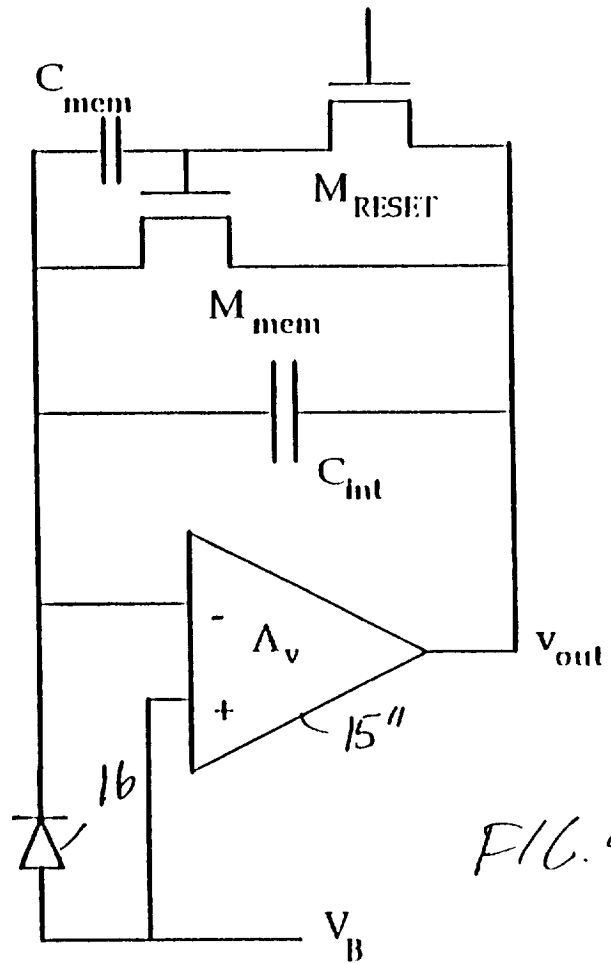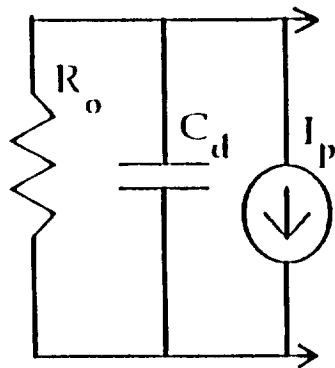Contact: John H. Kusmiss
Telephone No. 818-354-7770

FIG. 4a

$-A_v$ 15'

$h\nu$ 16

M_{inj}

I_{read}

C_{str}

V_{det}

V_p

FIG. 4b

M_{RST}

C_f

15''

NASA Case No. NPO-18518-1-CU
Page 3 of 8
SOLID-STATE IMAGE SENSOR WITH
FOCAL-PLANE DIGITAL PHOTON-
COUNTING PIXEL ARRAY
Inventor: Eric R. Fossum, et al.

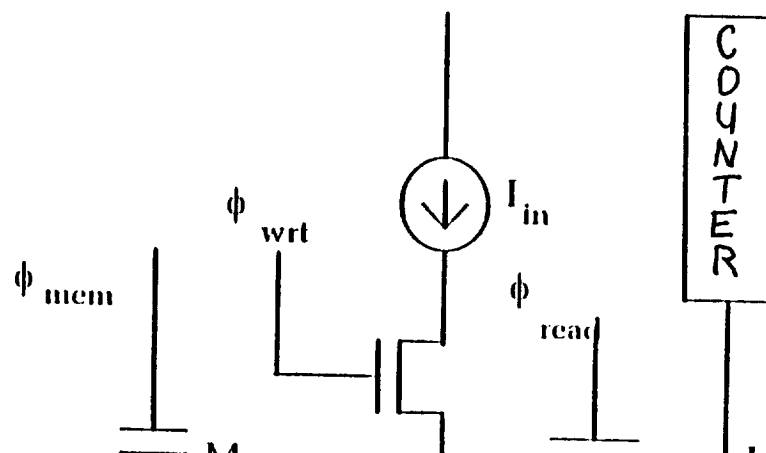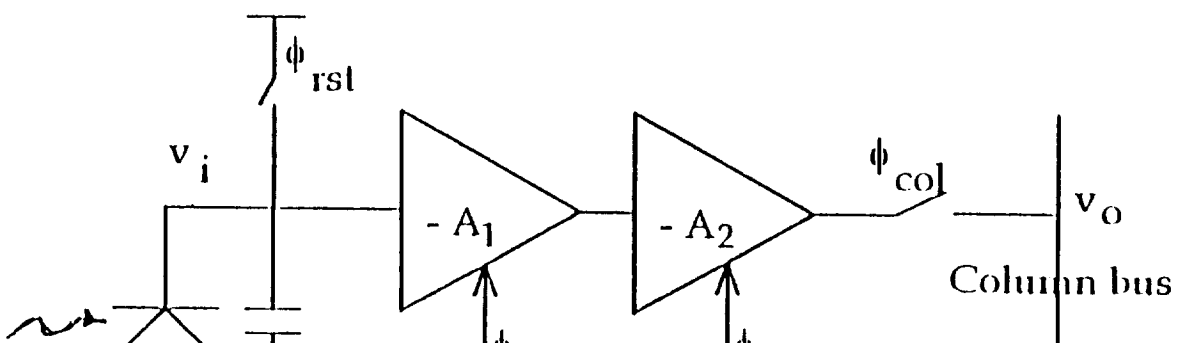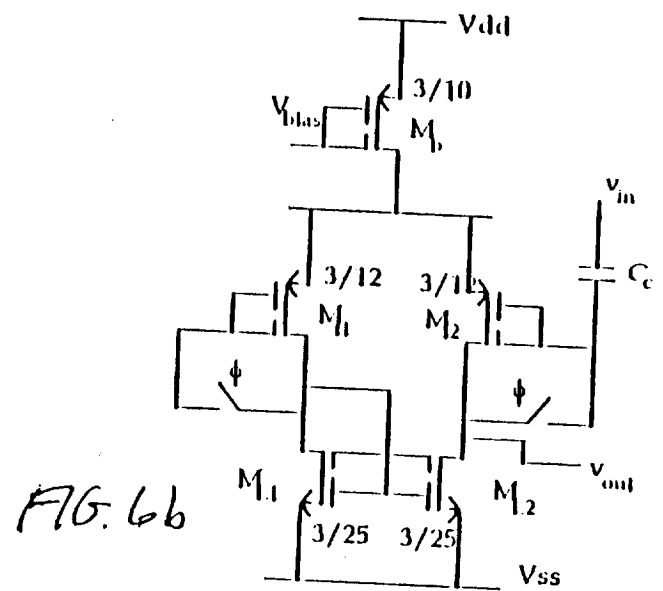Contact: John H. Kusmiss
Telephone No. 818-354-7770

FIG. 4C

The figure shows two circuit diagrams. The upper circuit (left in image) includes a current source I_p, a block labeled BDI, capacitors C_1 and C_2, a transistor M_{samp} with gate signal ϕ_{samp}, and an operational amplifier with $-$ and $+$ inputs and output v_{out}.

The lower circuit (right in image) is a small-signal model including current source i_p, conductance g_o, capacitor C_i, input voltage v_i, conductance g_f, capacitor C_f, current source $g_m v_i$, capacitor C_L, conductance g_{ds}, and output voltage v_{out}.
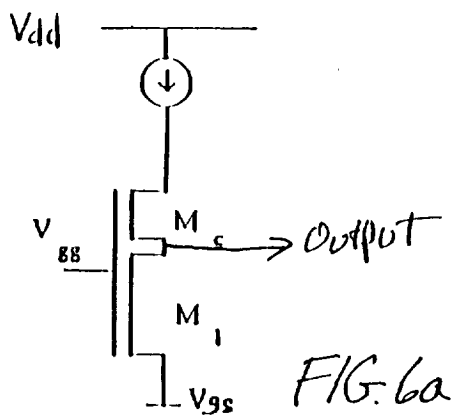
NASA Case No. NPO-18518-1-CU
Page 4 of 8
SOLID-STATE IMAGE SENSOR WITH FOCAL-
PLANE DIGITAL PHOTON-COUNTING PIXEL
ARRAY
Inventor: Eric R. Fossum, et al.

Contact: John H. Kusmiss
Telephone No.   818-354-7770

FIG. 5b

Equiv. Circuit of
Photodetector

FIG. 5a
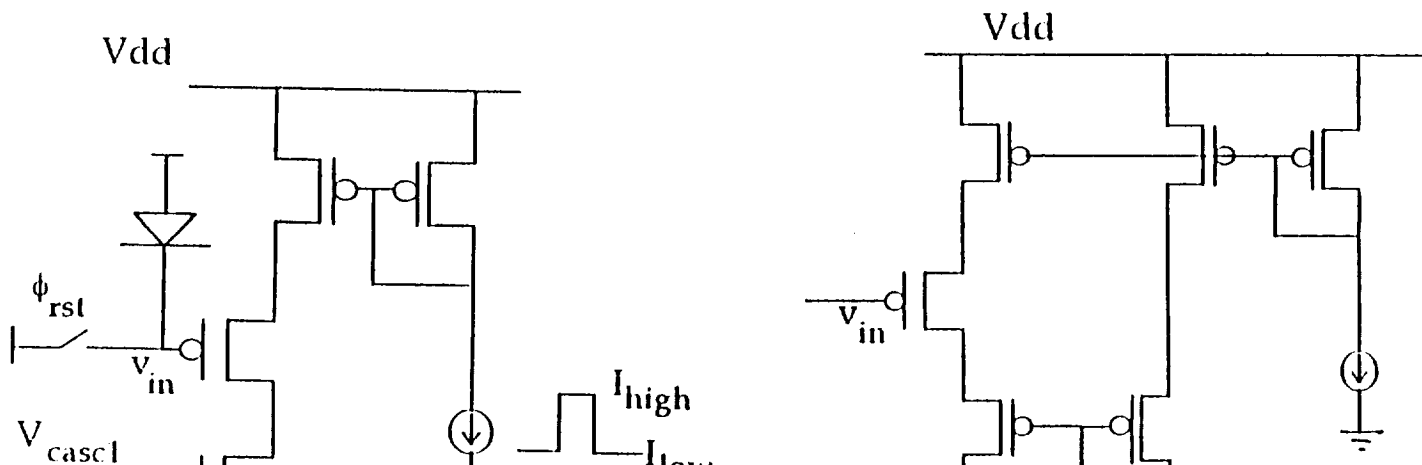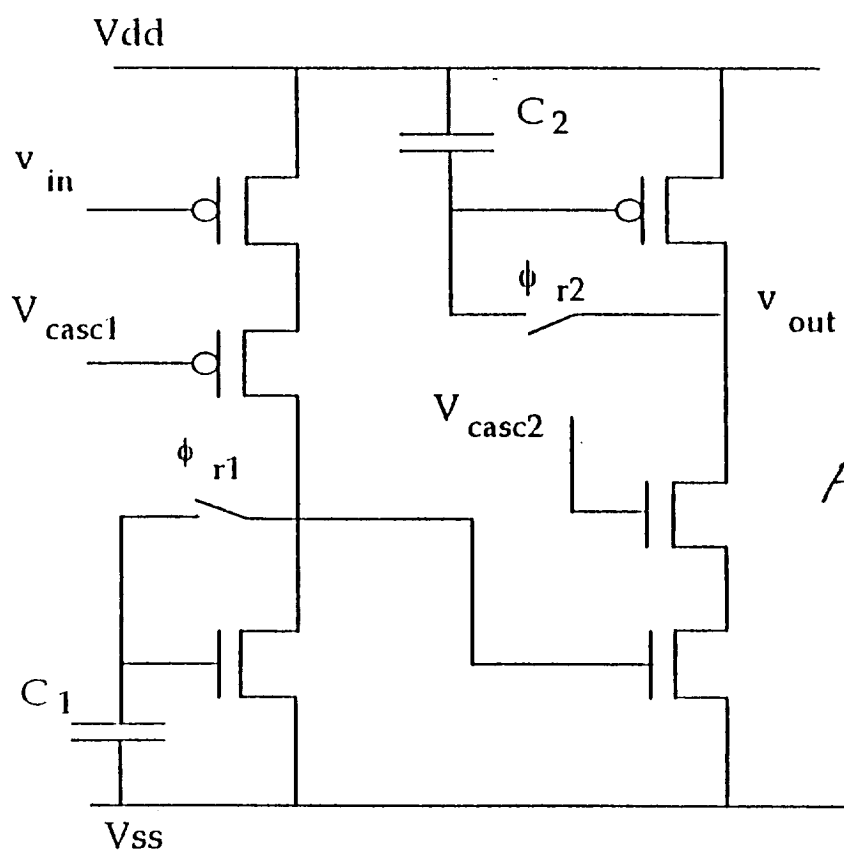
NASA Case No. NPO-18518-1-CU
Page 5 of 3
SOLID-STATE IMAGE SENSOR WITH
FOCAL-PLANE DIGITAL PHOTON-
COUNTING PIXEL ARRAY
Inventor: Eric R. Fossum, et al.

Contact: John H. Kusmiss
Telephone No. 818-354-7770

Vdd

V_{gg} M_s → Output

M_1

V_{ss} FIG. 6a

V_{bias} 3/10 M_b

Vdd

v_{in}

C_c

3/12 M_1 3/12 M_2

ϕ ϕ

v_{out}

M_{11} 3/25   3/25 M_{12}

Vss

FIG. 6b

ϕ_{rst}

v_i

$-A_1$ $-A_2$ ϕ_{col}

v_o

Column bus
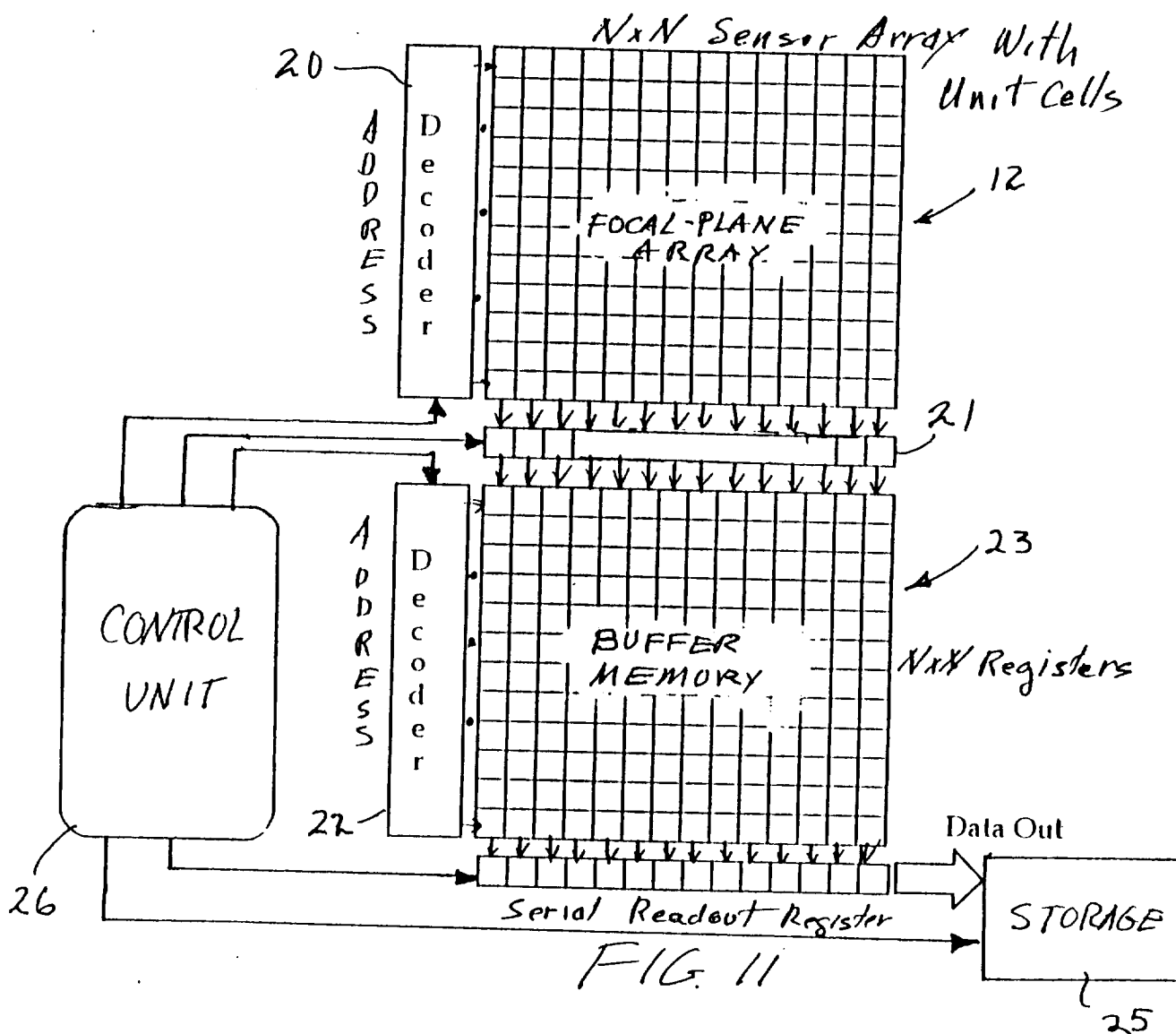
NASA Case No. NPO-18518-1-CU
Page 6 of 8
SOLID-STATE IMAGE SENSOR WITH
FOCAL-PLANE DIGITAL PHOTON-
COUNTING PIXEL ARRAY
Inventor: Eric R. Fossum, et al.

Contact: John H. Kusmiss
Telephone No. 818-354-7770

FIG. 8

NASA Case No. NPO-18518-1-CU
Page 7 of 8
SOLID-STATE IMAGE SENSOR WITH FOCAL-
PLANE DIGITAL PHOTON-COUNTING
PIXEL ARRAY
Inventor: Eric R. Fossum, et al.

Contact: John H. Kusmiss
Telephone No. 818-354-7770

FIG. 11

SOLID-STATE IMAGE SENSOR WITH
FOCAL-PLANE DIGITAL PHOTON-
COUNTING PIXEL ARRAY
Inventor: Eric R. Fossum, et al.

Contact: John Kusmiss
Telephone No. 818-354-7770